Spectral Heterogeneity of PRODAN Fluorescence in Isotropic Solvents Revealed by Multivariate Photokinetic Analysis

Brad A. Rowe, Carol A. Roach, Joanna Lin, Vincent Asiago, Olga Dmitrenko, and Sharon L. Neal*

Department of Chemistry and Biochemistry, University of Delaware, Newark, Delaware 19716

Received: March 14, 2008; Revised Manuscript Received: July 20, 2008

This paper describes a multivariate analysis of the fluorescence emission of 6-propionyl-2-dimethylaminonaphthalene (PRODAN) in a series of isotropic solvents of differing polarity and hydrogen-bonding ability. Multivariate methods distill the essential features from spectral data matrices so that the structural details that are embedded within the data are revealed to the analyst. In the aprotic solvents investigated, the analysis reveals a pair of emission components that have emission maxima that scale with the orientational polarizability. In the alcohols, short-lived, polarity-independent blue bands tentatively attributed to neutral hydrogen-bonded solute−solvent complexes form and relax prior to emission from paired bands that have Stokes shifts that scale with the solvent hydrogen-bonding ability rather than the polarity. In water, the short-lived blue bands were not observed, but the shift in the paired bands did scale with the solvent hydrogen-bonding ability.

Introduction

6-Propionyl-2-dimethylaminonaphthalene (PRODAN) was first synthesized by Gregorio Weber in 1979[1] as a probe of solvent polarity. Weber and Farris sought to impose polarity dependence on the emission of the molecule by maximizing the distance between the electron donor (dimethylamino) and electron acceptor (carbonyl) groups on the naphthalene scaffold. Indeed, the molecule exhibits dramatic solvatochromism: the emission maximum is near 394 nm (~25 380 cm^{-1}) in cyclohexane ($\varepsilon = 2.2$) and near 525 nm (~19 050 cm^{-1}) in water ($\varepsilon = 78.5$).[2] This property has lead many investigators to use PRODAN as a probe of local solvent polarity in microheterogeneous macromolecular systems. While there are reports of PRODAN being used to probe the conformation[3] and binding sites of proteins,[4] the probe has found more use in investigations of the nature and transitions of natural, synthetic, and biomimetic lipid membranes. Examples in this last group include research into the interfacial properties of ether lipids[5,6] alcohol interactions with biological membranes,[7] solute effects on phase transitions,[8] oxidative damage of phospholipids,[9] surface properties of cholesterol containing membranes,[10,11] water content of reverse micelles,[12] structure of interdigitated bilayers,[13] correlation of hydration to membrane curvature,[14] and fluidity of lipid mixtures.[15]

The wide use of PRODAN and its derivatives notwithstanding, consensus around a detailed description of the photokinetics of the chromophore has been elusive. The well-known dual fluorescence and structural similarity to dimethylaminobenzonitrile (DBMAN) led many to hypothesize that the dramatic increases in PRODAN transition wavelengths and Stokes shifts with solvent polarity were caused by solvent reorientation (relaxation) around a very large excited-state dipole generated by the formation of a twisted intramolecular charge transfer (TICT) excited state. In fact, several theoretical calculations supported this assignment.[16−19] However, Samanta and Fessenden performed transient dielectric loss measurements and determined that the change in the PRODAN dipole moment on excitation is far less than had been estimated.[20] Most importantly, Abelt and his coworkers synthesized constrained PRODAN derivatives that definitively establish the planarity of the charge transfer state.[21,22] While their work has not eliminated all discussion of the viability of the "twisted excited state" explanation,[23] the spectra emitted by the constrained twisted derivative indicate a minor, if any, role for a twisted excited state in PRODAN photokinetics. In fact, the most recent theoretical calculations support assigning PRODAN emission in homogeneous solvents to a planar excited state.[23]

Long before this recent work clarified the excited-state geometry, it was clear that something more than dipolar solvent relaxation was contributing to the stabilization of the PRODAN excited state. In dipolar solvent relaxation, the increase in emission wavelength and Stokes shift with polarity is a reflection of the reorientation of solvent dipoles around the dipole moment of the excited chromophore. This kind of nonspecific solvent effect can often be described by linear relationships between the Stokes shift and solvent polarizability.[2] When the viscosity of the solvent puts the rate of solvent reorientation on the scale of the fluorescence decay rate, it also produces a continuous red shift of the emission maximum from that of the Franck−Condon state to that of the solvent equilibrated state.[24] On the other hand, specific solute−solvent interactions, such as hydrogen bonding or complex formation, produce new emission bands that have longer wavelength maxima reflecting the thermodynamics of the interaction. A number of investigators have reported evidence of specific solvent interactions including multiple bands,[25] preferential solvation,[26] and protic effects.[27,28] One of the most compelling pieces of evidence that the PRODAN chromophore undergoes specific solvent interactions is the clear evidence of excited-state reactions that vary with emission wavelength and temperature in the decay of the PRODAN derivative LAURDAN in frozen and very cold ethanol.[29] It is also noteworthy that recent theoretical work supports a significant role for specific PRODAN solvent interactions. Artyukhov and coworkers[30] describe semiempirical calculations that reproduce PRODAN spectral properties in water within 5% when the hydronium ion was used as a complexing ligand. Recent

* To whom correspondence should be addressed. E-mail: sneal@udel.edu.

10.1021/jp802260y CCC: $40.75
Published on Web 12/05/2008

calculations at a much higher level of theory[23] included two hydrogen-bonded waters in the description of PRODAN in water but generated less accurate emission energies.

In spite of this long list of observations and calculations supporting specific interactions, it has not been easy to organize them into a simple formalism that rationalizes the Stokes shifts observed in various solvents. It is clear that hydrogen bonding as well as solvent reorganization around charge transfer species contribute to the Stokes shift, but the size of the shifts observed are not consistent with the excited-state dipole measurements (vide supra) or typical hydrogen-bond strengths. In water, the PRODAN Stokes shift is more than 7000 cm^{-1}, more than four times larger the value anticipated for typical hydrogen bonds.[31] One of the implicit features of earlier analyses of the relationship between PRODAN emission maxima and solvent properties is the expectation of a unimodal emission spectrum, dominated by contributions from a single state, in homogeneous solvents. However, the data collected in several of the specific interaction studies[25,29,32] consist of complex spectra that suggest a significant role for more than one excited state in PRODAN emission even in isotropic solvents. We hypothesize that resolution of PRODAN emission is essential to unraveling the mix of general and specific solute−solvent interactions producing PRODAN spectra.

This paper describes the collection and analysis of multivariate emission decays of PRODAN in homogeneous aprotic and protic solvents of varying polarity. Experimental methods to measure multivariate decays, also called wavelength-dependent emission decays or time-resolved fluorescence spectra, are well-established,[33,34] but data analysis methods which capitalize on the numerical structure of these data sets are still under development. In particular, advances in self-modeling methods,[35−38] which isolate characteristic data features and minimize the influence of analyst expectations on the results, can be invaluable in resolving complex spectra. The analyses described here use multivariate methods to determine the number of species contributing to the emission, distinguish dynamic Stokes shifts from photochemical conversions, and resolve overlapping spectral bands in multicomponent emission decays. Application of these tools to PRODAN emission in isotropic solvents produces results that suggest a photokinetic mechanism that rationalizes the scale of PRODAN Stokes shifts in protic solvents. The paper ends with a discussion of the implication of the results to larger issues in probe-based sensing, namely the applicability of this approach to understanding the photokinetics of other probes and the interpretation of probe behavior in microheterogeneous media.

Materials and Methods

Materials. 6-Propionyl-2-dimethylaminonaphthalene (PRODAN) was used as received (Molecular Probes, Eugene, OR). Stock solutions were prepared in HPLC-grade ethanol (200 proof, Pharmco, Brookfield, CT) and refrigerated in brown bottles for up to three months. Cyclohexane (certified A.C.S spectroanalyzed, Fisher Scientific, Pittsburgh, PA), cyclohexanol (99%, Sigma-Aldrich, St. Louis, MO), butanol (99%, Sigma-Aldrich, St. Louis, MO), and water (HPLC-UV grade, Sigma-Aldrich, St. Louis, MO) were used as received. Acetonitrile (HPLC grade, Fisher Scientific) and toluene (A.C.S certified, Fisher Scientific) were distilled in the presence of calcium hydride to remove trace impurities and water. PRODAN solutions were prepared by drying an aliquot of stock solution under an air-jet in a test tube overnight, then suspending the aliquot in solvent of interest to yield a final probe concentration of 2 μM. The dry acetonitrile and toluene samples were prepared in a glovebox under a nitrogen atmosphere. Fluorescence data acquisition was conducted with stirring under an argon atmosphere. All sample solutions were prepared fresh and used immediately.

Instrumentation. Pulsed excitation, provided by a mode-locked Ti:sapphire laser (Mira 900-F, Coherent, Santa Clara, CA) pumped by a 10 W Nd:YVO_4 frequency doubled laser (Millenia X, Spectra Physics, Mountain View, CA) generates the emission decay. The Ti:sapphire laser cavity is set to produce an 80 MHz train of ~150 fs pulses that is regulated by a frequency stabilization system (Mira Synchro-Lock, Coherent, Santa Clara, CA). The 80 MHz repetition rate of the pulse train is reduced to 5 MHz by a cavity dumper (Model 9200, Coherent, Santa Clara, CA). A beam splitter deflects a small portion of the excitation beam into an optical triggering unit (OCF-401-1, Becker & Hickl GmbH, Berlin, Germany), which is used to synchronize the detector system to the excitation pulse. The excitation beam frequency is adjusted by a harmonic generator (TP-1B fs Tripler, Uniwave Technology, Chatsworth, CA). The samples were excited at 375 nm using the frequency-doubled laser output. A Soliel-Babinet compensator (RC-10, Optics for Research, Caldwell, NJ) fixed the polarization of the excitation beam to vertical. Neutral density filters were placed in the path of the excitation beam to attenuate the power. The sample fluorescence is collected 90° to the excitation through a polarizer set to 54.7° from the vertical (magic angle) on an optical spectrofluorometer bench (K2, ISS, Champaign, IL). Collection of the sample fluorescence at the magic angle polarization setting avoids anisotropic effects on the fluorescence intensity produced by rotational motion of fluorophores in solution. In a few cases, a long-pass or bandpass filter is used to remove unwanted signals (e.g., large amounts of scattered excitation light). The sample emission is spectrally dispersed by a grating (150 groove/mm, blazed at 450 nm) spectrograph (HR320, Jobin Yvon Horiba, Metuchen, NJ). The spectrally dispersed fluorescence response is collected by a microchannel plate image intensifier (MCPII) (High Rate Intensifier, Kentech Instruments Ltd., South Moreton, U.K.) coupled to a CCD camera (Picostar HR 12, Lavision GmbH, Goettingen, Germany). Most images are acquired at a series of 0.1 ns intervals with respect to the excitation pulse under the control of a picosecond Delay Module (DEL-150, Becker and Hickl GmbH, Berlin, Germany). Variations to these acquisition properties are noted in the text. These images are stored on a computer that also controls the data acquisition system (image intensifier, CCD, delay module).

The probe absorption in the samples was checked using a diode array spectrophotometer (Hewlett-Packard/Agilent Technologies, Model 8452A, Palo Alto, CA).

Data Acquisition. The images collected by the CCD system at each time delay are integrated to generate the sample spectrum at each time step in the decay measurement. These spectra are collected and stored as a single matrix. A background offset was removed from the images, but they were not corrected for CCD quantum efficiency variations. All the image manipulation and data analysis (see below) routines used in this report were developed by the authors in the MATLAB programming environment (The Mathworks, Natick, MA).

Data Analysis. When the decay of a mixture of fluorophores is measured as a function of emission wavelength, it is convenient to store and analyze the data in matrix format. The details of these kinds of analyses are beyond the scope of this article and are provided as Supporting Information. The overview below describes the elements of the analysis of time-resolved emission decay matrices that are essential to interpretation of the results.

Each row of a time-resolved emission decay matrix (TR-EDM) is the decay measured at a different wavelength. Each column is the spectrum emitted by the sample at a different delay after excitation. Most importantly, the TR-EDM of a mixture is the sum of the matrices of the individual components and a matrix of the detector dark signal and other noise components. The component TR-EDMs are (outer) products of the respective emission spectra and decays of the individual components:

$$\mathbf{D} = \sum_{n=1}^{N} \mathbf{D}_{\bullet\bullet n} + \mathbf{E} = \sum_{n=1}^{N} \mathbf{x}_{\bullet n}\mathbf{y}_{\bullet n}^{\mathrm{T}} + \mathbf{E} = \mathbf{X}\mathbf{Y}^{\mathrm{T}} + \mathbf{E} \quad (1)$$

where $\mathbf{D}$ represents the $L \times T$ intensity matrix of the mixture, $\mathbf{D}_{\bullet\bullet n}$ represents the $L \times T$ intensity matrix contributed by the nth component, $\mathbf{E}$ represents the noise matrix, $\mathbf{x}_{\bullet n}$ is an L vector that represents the emission spectrum of the nth mixture component, and $\mathbf{y}_{\bullet n}$ is the T vector that represents the time domain emission decay of the nth component. The sets of component spectra $\{\mathbf{x}_{\bullet n}\}$ and decays $\{\mathbf{y}_{\bullet n}\}$ are stored on the columns of the matrices, $\mathbf{X}$ and $\mathbf{Y}$, respectively.

When the photokinetics are first order (i.e., characterized by constant rates) the component decay profiles, $\mathbf{Y}$, have simple structures. They can be described as combinations of monoexponential fundamental decays:

$$\mathbf{Y} = \mathbf{Z}\boldsymbol{\Gamma}\mathbf{W}^{\mathrm{T}} \quad (2)$$

where $\mathbf{Z}$ is a $T \times N$ matrix of the fundamental decays, $\boldsymbol{\Gamma}$ is an $N \times N$ matrix of concentration factors, and $\mathbf{W}$ is the $N \times N$ matrix that has eigenvectors of the photokinetic rate matrix, $\mathbf{K}$, along its columns. The fundamental decays are convolutions of the impulse responses of the sample components, which decrease monoexponentially at rates equal to the eigenvalues of $\mathbf{K}$ and the combination of the excitation and detector response functions. The eigenvector matrix, $\mathbf{W}$, defines the component decays by specifying the coupling of the fundamental decays.

Although emission decay matrices have simple linear structures in both dimensions, it is rare that the profiles of the pure component spectra or decays are located among the rows or columns of a TR-EDM. Consequently, mixture analysis consists of three stages: partitioning (factoring) of the matrix into a convenient pair of column and row basis sets, the estimation of the component responses, $\mathbf{X}$ and $\mathbf{Y}$, in terms of those basis sets, followed by characterization of the decays (i.e., identification of the photokinetic properties of the mixture components).

The first stage of TR-EDM analysis consists of factoring the matrix into a convenient set of column and row factors (basis vectors). There are an infinite number of such basis sets and most of them are not obviously related to the spectroscopic properties of the sample. The orthonormal factors generated by the singular value decomposition (SVD)[39] are among the most conveniently generated. The SVD computes the smallest set of column and row factors that describe the largest fraction of the data matrix variance:

$$\mathbf{D} = \sum_{p=1}^{P} \sigma_{pp}\mathbf{u}_{\bullet p}\mathbf{v}'_{\bullet p} = \mathbf{U}\boldsymbol{\Sigma}\mathbf{V}' \quad (3)$$

The product of the column factors, $\{\mathbf{u}_{\bullet \mathrm{p}}\}$, stored along the columns of $\mathbf{U}$, the row factors, $\{\mathbf{v}_{\bullet \mathrm{p}}\}$, stored along the columns of $\mathbf{V}$, and the intensity factors, $\{\sigma_{\mathrm{pp}}\}$, stored along the diagonal of the matrix $\boldsymbol{\Sigma}$ reconstructs the original matrix $\mathbf{D}$. The number of factors required to reproduce $\mathbf{D}$ is equal the smaller dimension of $\mathbf{D}$ ($P = \min(L, T)$) rather than N because $P-N$ components describe the variance of the random signals that come from instrument noise. A number of approaches to determining N, the number factors required to reconstruct the sample emission, have been described.[40−44] In the work described below, methods that estimate the number of factors based on the relative sizes of their magnitudes (singular values) and frequency content were used.

One of the advantages of matrix formatting is that the matrix factors reveal data features that can help the investigator identify various types of system behavior. In this work, the differences that general and specific solute−solvent interactions can impose on fluorescence decays can be observed in the orthogonal factors when the data are acquired with sufficient temporal resolution. These differences are consequences of the numerical distinctions between dynamic Stokes shifts and superposition of overlapping bands in complex spectra. These differences, in the number and complexity of the spectral shapes required to reconstruct data matrices, are features that the analyst may use to distinguish general and specific solvent interactions.

In the case of specific solute−solvent interactions, the spectral profile at any time after excitation can be described by a linear combination of a small number of spectral components and a small factor that has a random profile associated with measurement error. In the case of general solvent relaxation at rates comparable to the acquisition time, the spectral profile at each time point after the first has a similar shape but is shifted on the wavelength axis. Since most general solvent relaxation processes occur on the picosecond time scale,[28] this phenomenon is only likely to be observed in viscous solvents using the apparatus described above. Examples of the two cases have been simulated and are presented in Figure 1. The left column (Figure 1A−D) depicts the orthonormal factorization of a matrix constructed to simulate the emission of a solute that exhibits specific solute−solvent interactions. The right column (Figure 1E−H) depicts the factorization of a matrix constructed to simulate the dynamic Stokes shift associated with continuous dipolar relaxation. The spectral profile at each time point after the first is a nonlinear function of the earlier spectra, which requires a much larger number of components (more than 15 in the example in Figure 1E−H) to reconstruct in the linear framework of the singular value decomposition. The profiles of the 5th through 15th row and column basis sets are not shown, but the trends in the shapes are predictable: the basis vectors exhibit increasingly higher frequency baseline oscillations.

In the work reported here, the first stage of mixture TR-EDM analysis is not completed by calculation of the orthogonal factors. We have found decomposition into more physically relevant, and thus visually meaningful, basis sets helpful for analyzing highly overlapped decay data. We call this decomposition the photokinetic matrix decomposition (PMD) because it factors first order TR-EDMs into combinations of dynamically linked spectra and fundamental (monoexponential) decays:

$$\mathbf{D} \approx \sum_{n=1}^{N} \gamma_{nn}\mathbf{s}_{\bullet n}\mathbf{z}'_{\bullet n} = \mathbf{S}\boldsymbol{\Gamma}\mathbf{Z}' \quad (4)$$

where the columns of $\mathbf{S}$ and $\mathbf{Z}$ are photokinetically informative factors of the columns and rows of $\mathbf{D}$, respectively, and $\boldsymbol{\Gamma}$ is a diagonal matrix of relative intensity factors. In eq 4 the P-N factors associated with the measurement error have been deleted from the analysis. In other decay analysis methods, such as global analysis.,[45,46] experimental decay data also are described in terms of dynamically linked spectral and monoexponential decay basis vectors. The dynamically linked spectral vectors are often called decay associated spectra (DAS) to distinguish them from species associated, i.e., component, spectra, and the monoexponential decays are called fundamental decays. We use similar notation and nomenclature, but there is an important difference between PMD and procedures such as global analysis.

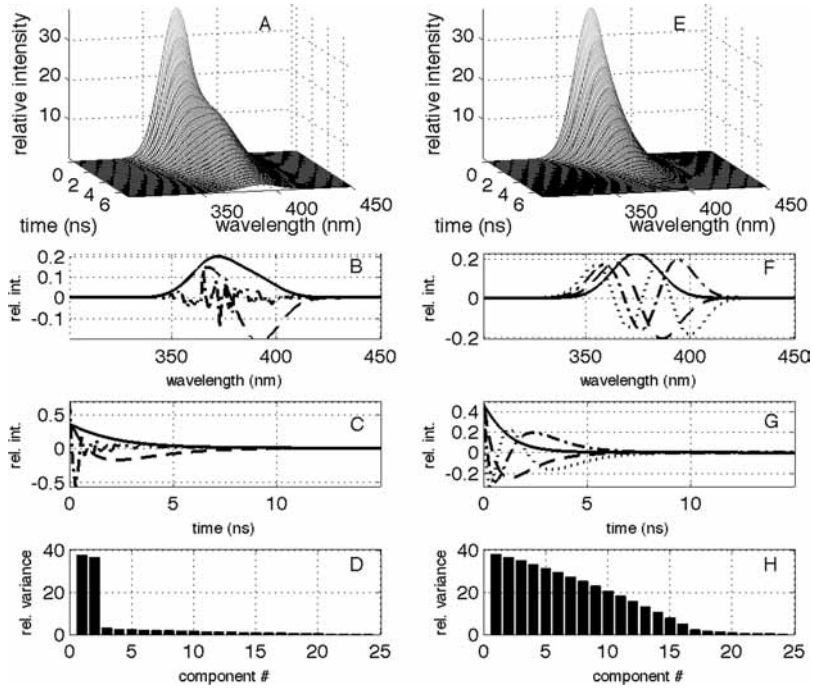

Figure 1. Orthogonal decomposition of matrices simulating solvent relaxation: (A) TR-EDM modeled to illustrate specific solvent interaction exhibiting two spectral components; (B) First three column (spectral) orthogonal basis (singular) vectors of TR-EDM in A; (C) First three row (temporal) orthogonal basis (singular) vectors of TR-EDM in A; (D) Relative variance of orthogonal components of TR-EDM in A; (E) TR-EDM modeled to illustrate general solvent interaction; (F) First four column (spectral) orthogonal basis (singular) vectors of TR-EDM in E; (G) First four row (temporal) orthogonal basis (singular) vectors of TR-EDM in E; (H) Relative variance of orthogonal components of TR-EDM in E.

In the decomposition, the fundamental decays are solutions of a generalized eigenvalue problem formulated from the data matrix. This procedure is a variant of the DECRA method described by Windig for analyzing pulsed gradient spin echo (PGSE) nuclear magnetic resonance measurements.[47,48] Both methods (i.e., PMD and DECRA) exploit the self-similarity of exponential decays across the measurement (see Supporting Information for details). This means that these basis vectors are not located by an optimization routine and so are not subject to the ambiguity inherent in fitting multiexponential decays but, within limitations imposed by instrument time constants and measurement error, are self-modeling, i.e., characteristic of the data matrix structure produced by the excited-state dynamics of the sample. The maximum entropy method,[49,50] which computes distributions of the most probable decay constants from decay profiles, may also be considered self-modeling, but as it is commonly used, it is applied to individual decays and includes no mechanism for preserving the correlations observed across the wavelength domain in TR-EDMs.

In the second stage of the mixture analysis, a curve resolution algorithm is used to determine the component responses (i.e., spectra and intensity decay profiles) associated with the mixture components from the matrix factors. A number of algorithms for this problem have been described.[35,36,51,52] Most of them involve transforming the orthonormal factors to component responses using optimization routines to find factor transformations that avoid physically untenable properties in the response (i.e., negative intensities). These algorithms may also impose regularizing constraints on the transformation to generate a single solution because an infinite number of factor combinations potentially represent spectra. Positive matrix factorization and alternating least-squares approaches are among the most widely cited methods.[53,54] In the work reported here, a curve resolution algorithm that uses constraints to incorporate a priori knowledge regarding the properties of the component responses into the transformation of the fundamental factors is used. The algorithm also tailors the optimization function to regularize the solution using spectral smoothness and/or dissimilarity. The algorithms select solutions as close as possible to the fundamental factors while avoiding physically untenable response properties. This criterion imposes a reference on the results that facilitates comparisons of factors resolved from related data matrices. Additional details concerning the algorithm are provided in the Supporting Information. The estimates of the component responses are

$$\hat{\mathbf{X}} = \mathbf{S}\hat{\mathbf{\Pi}}$$
$$\hat{\mathbf{Y}} = \mathbf{Z}\mathbf{\Gamma}\hat{\mathbf{\Pi}}^{-1} \quad (5)$$

where $\hat{\mathbf{\Pi}}$ transforms the decay associated spectra, $\mathbf{S}$, to component spectra estimates, $\hat{\mathbf{X}}$ Comparing eqs 1, 2, and 4 shows that $\hat{\mathbf{\Pi}}$ is the inverse of $\mathbf{W}$, the transfer (rate) eigenvector matrix.

In the final stage of the matrix analysis, the photokinetic properties of the mixture components are computed from the component responses. The most important of these are the photokinetic rates collected in the transfer matrix, $\mathbf{K}$, and the initial intensities, $\mathbf{y}_0$, given by

$$\mathbf{K} = \hat{\mathbf{W}}\mathbf{\Lambda}\hat{\mathbf{W}}^{+}$$
$$\mathbf{y}_0 = \hat{\mathbf{W}}\gamma \quad (6)$$

where the columns of $\hat{\mathbf{W}}$ are the transfer (rate) matrix eigenvectors, the diagonal elements of $\mathbf{\Lambda}$ are the transfer (rate) matrix eigenvalues, and the elements of γ are the intensity factors of the components. These properties may be calculated algebraically from the fundamental factors and component responses using procedures described in the Supporting Information.

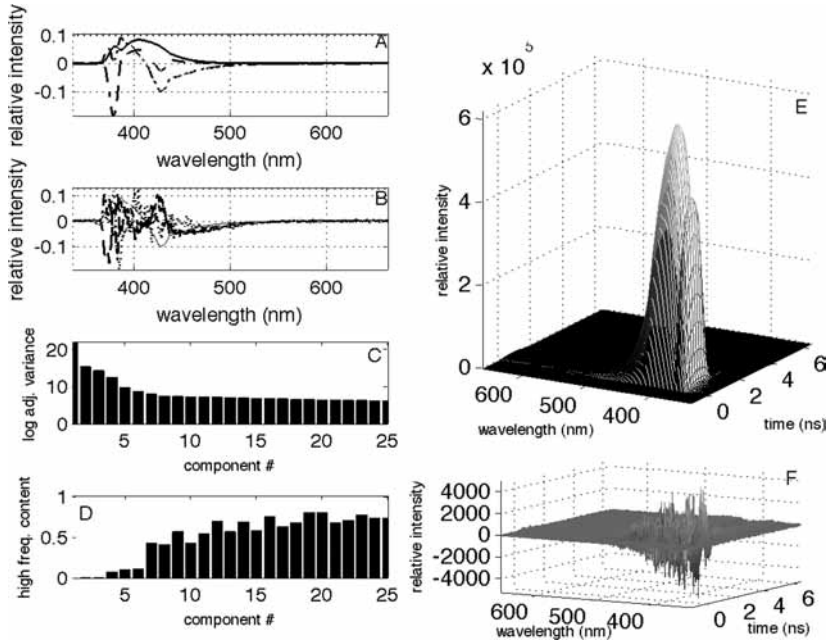

Figure 2. Orthonormal factors of 2 μM PRODAN in cyclohexane TR-EDM: (A) First three column (spectral) singular vectors of TR-EDM, first (solid line) captures more variance than second (dotted line) and so on; (B) Third through sixth column (spectral) singular vectors of TR-EDM; (C) First 25 reduced eigenvalues; (D) Fraction of Fourier transform components above noise threshold for each column (spectral) singular vectors; (E) TR-EDM reconstructed from first three principal components; (F) Residual of original matrix not included in reconstruction.

Computational Methods. Quantum chemistry calculations were carried out using the Gaussian03 program system[55] utilizing gradient geometry optimization.[56] Most of these calculations were performed using GridChem computational resources and services (www.gridchem.org).[57] All geometries were optimized using the B3LYP[58,59] and hybrid meta MPWB1K[60] functionals with 6-31G(d) and 6-311+G(d, p) basis sets.[61] Vertical energies of the singlet excited-state transitions were calculated using the time-dependent density functional theory method (TD-DFT).[62−64] Solvation corrections and optimizations in dielectric media with cyclohexane and methanol dielectric constants were made using the conducting polarized continuum model (CPCM)[65,66] implemented in Gaussian 03. For TD calculations, we employed the same method used in the structure optimization.

Results and Discussion

The analysis of an experimental PRODAN TR-EDM begins with the calculation of the orthonormal factors. This enables the analyst to estimate the number of fluorescent species contributing to the data matrix and look for evidence of general solvent relaxation. Figure 2 illustrates the orthonormal factors of the TR-EDM of 2 μM PRODAN in cyclohexane collected in 0.05 ns intervals. Figure 2A and B shows the first six orthonormal spectral (column) factors of the matrix. The first three factors are very smooth while the next three exhibit substantial random fluctuations. Figure 2C depicts the relative contribution (reduced eigenvalue[41]) that the first 25 factors (see eq 3) make to the matrix. The amplitudes of the first three factors are somewhat larger than the next three, which are slightly larger than the remaining components. This result suggests that the first three components are very likely to contribute to the fluorescence signal but is equivocal regarding the source (signal vs noise) of the next three factors. Figure 2D shows the results of a Fourier transform-based rank analysis.[43] This panel shows the relative contribution of pure oscillations that have frequencies higher than 20% of the Nyquist frequency to each of the first 25 spectral factors. These results agree with the amplitude-based analysis. The high frequency content of the fourth through sixth components is much smaller than that of the remaining components but not as low as the first three components. Figure 2E shows the matrix reconstructed using the first three orthonormal factor products. Figure 2F depicts the residuals of the TR-EDM after the reconstructed matrix was subtracted from the experimental data. The residuals are consistent with the measurement: they are largest at those points at which the intensity of the original matrix is largest as expected for signals distorted by photon statistical noise. While it is not surprising that these rank analysis results are not definitive, the question remains how many emission components contribute to the data matrix?

The other motivation for inspecting the orthonormal factors of the TR-EDM is to look for evidence of dynamic Stokes shifts in the data. When they are present, low amplitude factors show baseline oscillations that are large compared to the measurement error (see Figure 1 for illustration.) These oscillations generally extend the spectral response across the wavelength domain. This is distinct from the localization observed in factors that reflect the presence of photon statistical noise and scattering or other background signals. By these criteria, the fourth through sixth factors do not exhibit evidence of general solvent relaxation; the emission components in these factors are nearly superimposable. The relatively large amplitude and smoothness of the fourth through sixth factors is likely a reflection of the size and fluctuation in the scattering bands contributing to the data set.

The orthonormal factors depicted in Figures 1 and 2 illustrate the challenge of using this basis set to determine the component responses. After close inspection, one might be convinced that these factors are linear combinations of the component responses, but most would be hard pressed to surmise the shape of the component responses from orthonormal factors. Figure 3 illustrates the partitioning of the TR-EDM of 2 μM PRODAN in cyclohexane (depicted in Figure 2) into component responses via fundamental factors generated using the photokinetic matrix decomposition. While it was difficult to determine if the fourth

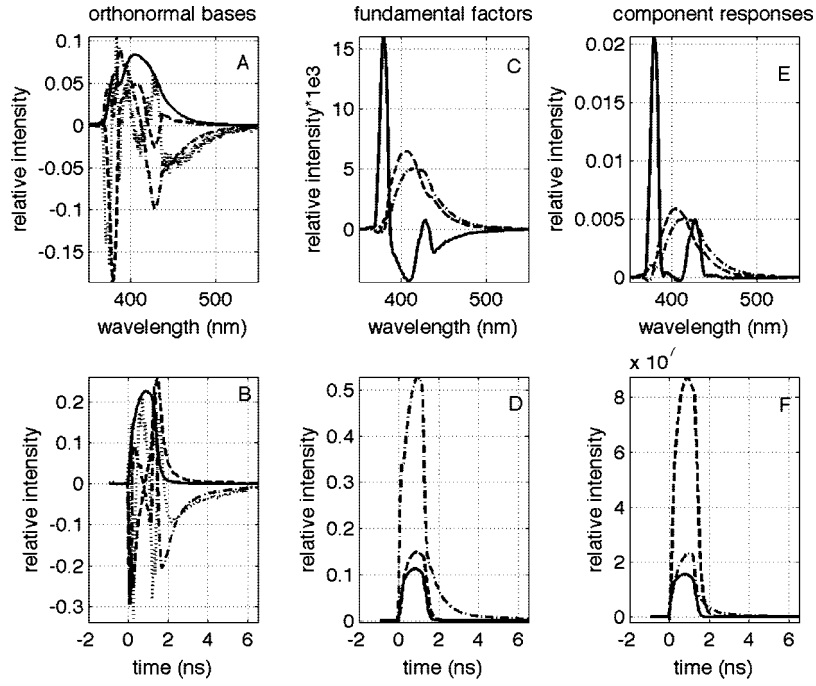

Figure 3. Stages of matrix partitioning: (A) First four column (spectral) singular vectors of TR-EDM of PRODAN in cyclohexane; (B) First four row (decay) singular vectors of TR-EDM; (C) Decay associated spectra of TR-EDM of PRODAN in cyclohexane; (D) Fundamental decays of TR-EDM of PRODAN in cyclohexane; (E) Estimated spectra of PRODAN components in cyclohexane; (F) Estimated decay profiles of PRODAN components in cyclohexane.

through sixth orthonormal factors contribute to the signal variance of the matrix, the content of the fundamental factors are much more amenable to visual inspection. It is clear from the results of the photokinetic matrix decomposition that the TR-EDM of PRODAN in cyclohexane consists of three emission components. Using more than three components in the photokinetic decomposition of this matrix generates complex factors as measurement error is incorporated into the temporal (row) factors as oscillations. The three fundamental factors are shown in Figure 3C and D. The first spectral (column) fundamental factor combines features of elastic and inelastic scattering with fluorescence features. The corresponding temporal (row) factor is the narrowest of the three and is similar to the profiles of reference scatterrers (data not shown), so both factors (column and row) are designated scattering fundamental factors. The negative bands in the spectral scattering factor reflect the strong temporal overlap of the scattering profile with the fluorescence decay profiles rather than a photochemical interaction between these components. The other two fundamental factors (dashed and dot-dashed profiles in Figure 3C) capture distinct fluorescent components, as evidenced by their corresponding decay profiles. These factors (column and row) are called fluorescence fundamental factors. The absence of overlapping negative bands in the fluorescence fundamental factors indicates that the two species in this sample experience limited excited-state interaction. In this case, predicting the component responses from the fundamental factors is straightforward; the fluorescence fundamental factors provide good estimates of the component spectra. It is almost possible to predict the scattering spectrum from the fundamental factors by inspection. The transformation from Figure 3C to E clearly requires adding some fraction of the fluorescence fundamental factors to the scattering factor. The sample components have short decay times so the decay profiles, which are convolutions of the instrument response and the impulse responses of the sample components, are dominated by the instrument response, which has a substantial width relative to the decays of these components. Figure 3 also illustrates the different normalization conventions that were used for the matrix factors. By definition, the orthonormal factors are scaled to unit length (squared values sum to one). The fundamental factors are normalized so that the intensity factor, γ_{nn}, for each component reflects the number of fluorophores rather than the spectrum or decay profile breadth. The spectral factors are scaled so that their absolute values sum to unity, while the fundamental decay factors are scaled so that their value at the excitation pulse maximum is unity, before an adjustment for the width of the instrument response profile. When a matrix is partitioned into component responses, the spectral responses are normalized so that their values sum to unity. In order to approximate the data matrix, the decays must be scaled so that their intensities reflect the relative magnitude of the components in the data matrix.

The results of multivariate analysis of TR-EDMs of PRODAN in three aprotic solvents are depicted in Figure 4. In each case, the photokinetic decomposition generated fundamental factors similar to those shown in Figure 3: one component that combines scattering and fluorescence and two fluorescence components that exhibit monoexponential decays. The fluorescence fundamental factors indicate that the corresponding excited states decay with limited interaction. The fluorescence contributions to the scattering factors are distinct and easily removed by combination with one or both of the fluorescence fundamental factors.

Solvent Raman bands are evident in the scattering spectra of cyclohexane and acetonitrile. None of the spectra exhibit evidence of dynamic Stokes shifts. The observation of two emission bands is consistent with the presence of two distinct bands reported in several theoretical and experimental investigations of PRODAN absorption transitions.[18,19,21,67,68] Definitive assignments of these bands have not been reported, but the variation in emission wavelength from both states with solvent polarity indicates that both have substantial charge transfer character. It is noteworthy that the redder spectrum decays at the slower rate and is more intense than the blue component in

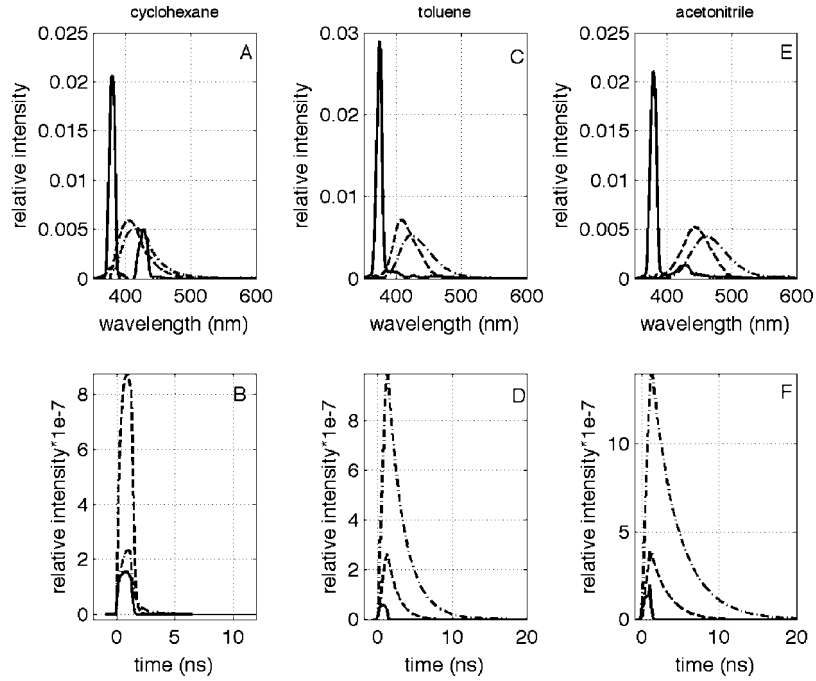

Figure 4. Component responses of PRODAN in aprotic solvents: (A) Estimated spectra of PRODAN components in cyclohexane; (B) Estimated decay profiles of PRODAN components in cyclohexane; (C) Estimated spectra of PRODAN components in toluene; (D) Estimated decay profiles of PRODAN components in toluene; (E) Estimated spectra of PRODAN components in acetonitrile; (F) Estimated decay profiles of PRODAN components in acetonitrile.

toluene and acetonitrile. Additionally, the red bands have peak maxima approximately 15 nm longer than the blue bands in all three solvents. The variation of the emission maxima of both components with solvent polarity is shown graphically in Figure 6A. Here, the photokinetics produce bands that have Stokes' shifts that are linear with respect to the modified solvent orientational polarizability,[2] which is also called the polarity function. The modified orientational polarizability is defined within the Onsager reaction field model of the solvent by

$$\Delta f' = \frac{\varepsilon - 1}{2\varepsilon + 1} + \frac{n^2 + 1}{4n^2 + 2} \tag{7}$$

The TR-EDMs of PRODAN in protic solvents are more difficult to analyze, and the results are more intriguing. The fluorescence fundamental factors generated by the photokinetic decomposition show clear evidence of substantial excited-state interaction. In most cases, the component responses were computed from the fundamental factors using the curve resolution algorithms outlined in the Data Analysis section, but the coefficients that relate the fundamental factors to the spectra in butanol were determined heuristically as described above for the case of PRODAN in cyclohexane in Figure 3C and E. Component responses that were resolved from the TR-EDMs of PRODAN in cyclohexanol, butanol, ethanol, and water are shown in Figure 5. In each solvent, a pair of red-shifted bands similar to those observed in the aprotic solvents was resolved from PRODAN emission. As before, the bands were on the order of 15 nm apart, and the emission maxima of both bands increase with solvent polarity. In every case except water, the redder band is slower and substantially more intense. It also is important to note that the emission maxima of the red-shifted bands do not depend linearly on the orientational polarizability of the solvent as those observed in the aprotic solvents do (see insert of Figure 6B). In cyclohexanol, PRODAN emission exhibits baseline oscillations indicative of the dynamic Stokes shifts expected in this viscous solvent. These lead to small, negative red-shifted bands in one of the component spectra.

PRODAN emission in the protic solvents exhibits other features that are quite different from those observed in aprotic solvents. All the alcohols emit at least one short-lived blue band in addition to the red-shifted pair. PRODAN emission in cyclohexanol ($\varepsilon = 15.0$, $\eta = 57.5$ cP) includes blue bands from two relatively short-lived states. In butanol ($\varepsilon = 17.8$, $\eta = 2.9$ cP), only one blue band can be resolved from the PRODAN emission. Since the emission maximum wavelength is the average of the two bands observed in cyclohexanol and the decay time is close to the limit of the apparatus, it is possible that this band is a superposition of two bands analogous to those observed in cyclohexanol. In ethanol ($\varepsilon = 24.3$, $\eta = 1.1$ cP), a blue band is observed at essentially the same wavelength, but its decay time is so short that it cannot be resolved from the scattering component. Here too, instrument limitations may obscure a second blue band. The excited-state species associated with these bands do not exhibit charge transfer character; that is, their emission maxima do not change with solvent polarity, but their decay rates increase with the solvent polarity. Definitive assignment of these bands will require further study, but the location and dynamics (off-diagonal elements of **K** in eq 6, Supporting Information, Table S1) of these bands lead us to speculate that a neutral PRODAN−solvent complex that is consumed as charge transfer occurs emits these bands. This interpretation is bolstered by the correlation of the emission maxima of the red-shifted charge transfer bands to the hydrogen-bonding component of the cohesive energy density (i.e., Hansen's parameter,[69] δ_H) of the protic solvents as shown in Figure 6B (average correlation coefficient equal to 0.99 as compared to 0.94). This dependence suggests that charge transfer strengthens hydrogen bonds between solute and solvent, a mechanism that has been invoked to describe the spectroscopy of other probes.[70]

The obvious question is whether these results shed any light on the nature of the emitting states. The consistent observation of pairs of bands is supported by density functional theory/single excitation configuration interaction (DFT/SCI) calculations

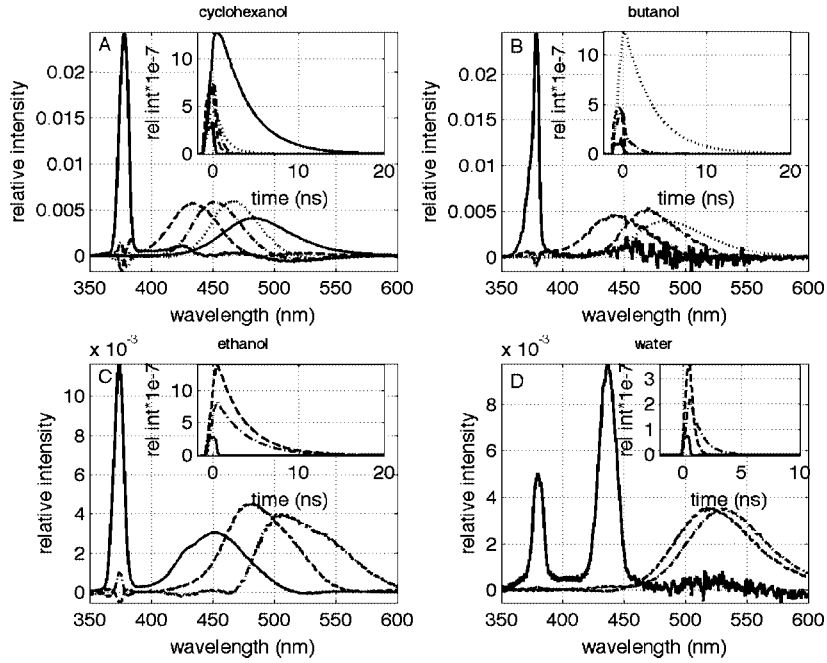

Figure 5. Component responses of PRODAN in protic solvents: (A) Estimated spectra of PRODAN emission components in cyclohexanol; (A, insert) Estimated decay profiles of PRODAN emission components in cyclohexanol; (B) Estimated spectra of PRODAN emission components in 1-butanol; (B, insert) Estimated decay profiles of PRODAN emission components in 1-butanol; (C) Estimated spectra of PRODAN emission components in ethanol; (C, insert) Estimated decay profiles of PRODAN emission components in ethanol; (D) Estimated spectra of PRODAN emission components in water; (D, insert) Estimated decay profiles of PRODAN emission components in water.

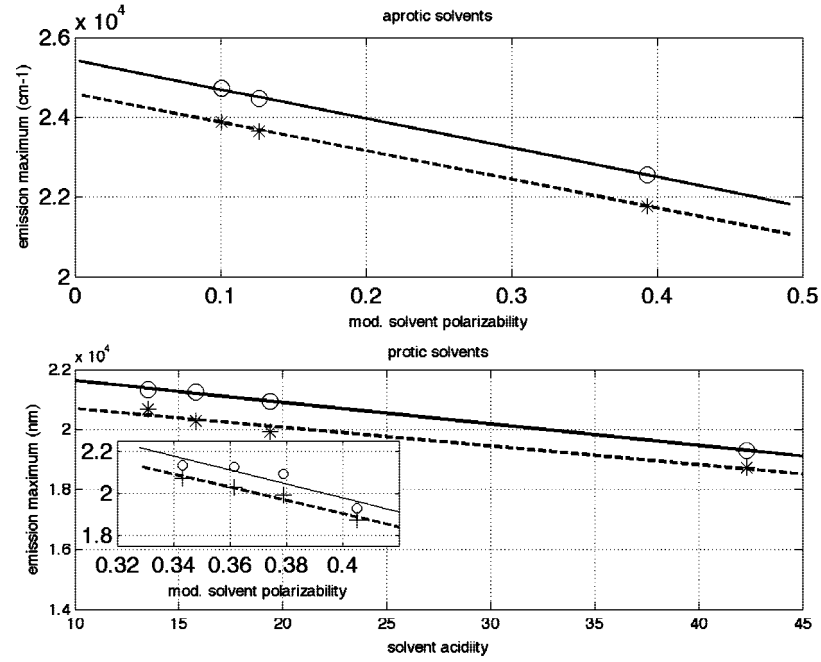

Figure 6. Emission maximum analysis: (A) Plot of PRODAN emission maxima dependence on modified solvent polarizability ($f(n, \varepsilon)$) in aprotic solvents; (B) Plot of PRODAN charge transfer emission maxima dependence on Hansen hydrogen bonding parameter (∂_h) in protic solvents; (Insert) Plot of PRODAN charge transfer emission maxima dependence on modified solvent polarizability ($f(n, \varepsilon)$) in protic solvents.

reported a decade ago by Parusel et al.[18] They assign the two absorption bands to close lying, strongly coupled $\pi \rightarrow \pi^*$ transitions to excited states of A′ symmetry. Their orbital analysis and dipole moment calculations led them to characterize these states as intramolecular charge transfer states. Such states are expected to exhibit the polarity-dependent red shifts we observed in aprotic solvents. Neither the recently published[23] nor our own time-dependent density functional theory (TD-DFT) calculations using the B3LYP functional find comparable oscillator strengths for S1 and S2 (nor evidence of such strong coupling in S1 and S2; see Supporting Information, Table S3). However, our results using the MPWB1K functional, reported in Table 1, indicate substantial oscillator strength for the S2 excitation, which is close in energy (0.23 eV higher, gas phase) to S1. The molecular orbitals calculated by using both, B3LYP and MPWB1K methods, are similar to those described by Parusel and coworkers.[18] TD B3LYP and TD MPWB1K calculations indicate that S1 is the HOMO⇒LUMO transition and S2 is a combination of the (HOMO−1)⇒LUMO and HOMO⇒(LUMO+1) transitions (see Supporting Information,

TABLE 1: Singlet-Singlet Excitation Energies (E, eV) and Oscillator Strengths (f_{osc}) Calculated at the TD MPWB1K/6-311 + G(d, p) + PCM (Solvent = Cyclohexane, Methanol) Level of Theory[a]

	gas phase		cycloxehane		methanol	
state	E	f_{osc}	E	f_{osc}	E	f_{osc}
S1	4.00 (311.6 nm)	0.29	3.83 (323.8 nm)	0.50	3.74 (332.0 nm)	0.55
S2	4.23 (293.3 nm)	0.11	4.14 (299.4 nm)	0.13	4.07 (305.0 nm)	0.12
S3	5.05 (245.3 nm)	0.48	4.89 (253.5 nm)	0.59	4.83 (256.7 nm)	0.43
S4	5.51 (224.9 nm)	0.45	5.38 (230.6 nm)	0.72	5.35 (231.8 nm)	0.62

[a] Structures were optimized at the MPWB1K/6-31 + G(d, p) + PCM level of theory.

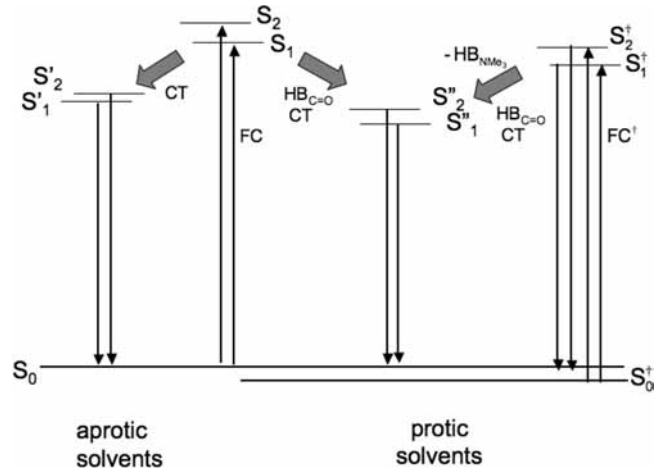

Figure 7. Possible PRODAN photokinetic scheme.

Figure 1S and additional details). Interestingly, the DFT/SCI calculations[18] assigned only HOMO⟹(LUMO+1) character to S2. Both S1 and S2 have substantial charge transfer character as the electron density around the amino group is reduced and that around the carbonyl oxygen increases in both transitions. It is important to note that the (HOMO−1)⟹LUMO excitation contributing to S2 in our calculations has the largest change of the electron density on the oxygen (compare orbitals 60 and 62 in Figure 1S in the Supporting Information). This may result in a larger probability of carbonyl oxygen protonation upon excitation to the S2 excited surface. However, the energies of these transitions do not agree with experimental values as well as the DFT/SCI calculations.[18]

The observation of neutral probe−solvent complexes with energies near 2.75 eV is partially supported by the recent reports[23] by Mennucci et al. in which water association was explicitly included. These authors report a calculated value for S1⟹S0 of PRODAN in water medium at 2.77 eV at the TDB3LYP level of theory when polarizable continuum modeling is used to represent the solvent. When two hydrogen-bonded water molecules were added to the PRODAN molecule, they found a value of 2.61 eV for this transition, supporting the association of H-bonding with red-shifted emission. None of the calculations reported to date explain the short-lived blue bands we observed experimentally in addition to the red-shifted pair in alcohol solutions. One explanation that integrates the evidence in our calculations suggesting excitation increases the probability of carbonyl oxygen protonation with the evidence that the species emitting the blue bands are in equilibrium with and/or being converted to those emitting the red bands, involves formation of three excited species: one produced by excitation of PRODAN molecules hydrogen bonded to the solvent at the amino group in the ground state and two produced by excitation of PRODAN molecules, which then are protonated at the carbonyl. In this picture, amino-protonated excited states dissociate prior to charge transfer and carbonyl protonation. The amino-protonated species have emission maxima that do not respond to solvent polarity while the carbonyl-protonated species have energies that depend on the hydrogen-bonding ability of solvent as we observed and reported in Table 2 and Figure 6B. A scheme depicting these processes is in Figure 7.

The solvatochromic shift of PRODAN has been difficult to characterize because the position of the electron donor and acceptor substituents contributes to a substantial redistribution of the molecule's electron density on excitation. When these functional groups are hydrogen-bond donors or acceptors, as they often are, excitation changes their hydrogen-bonding characteristics with the electron distribution. Maciejewski and coworkers[70] reviewed these issues as they apply to 4-aminophthalamide (4-AP). They point out that the impact of electronic redistribution is often overlooked in the analysis of probe emission but that many investigators have reported that probe molecules with donor and acceptor groups often form hydrogen bonds with several solvents.[27,28,71−74] Taken together, these precedents and our results suggest that the dramatic stabilization of PRODAN excited states in protic solvents may be attributed to combination of hydrogen bonding and charge transfer effects. Maciejewski and coworkers also conclude that combination of general and specific probe−solvent interactions complicate a probe's use in solvatochromic studies. As long as the probe response to specific interactions can be resolved from that of general interactions these complications may be circumvented. The need to distinguish probe interaction type as well as probe responses to medium microenvironments can make characterization of microheterogeneous media especially difficult. The results presented in this report demonstrate that PRODAN molecules in polar aprotic microenvironments can emit spectra

TABLE 2: Emission Maxima (λ_{max}) and Apparent Decay Times (τ) of PRODAN Components in Isotropic Solvents of Varying Solvent Polarizability ($\Delta f'$) and Hydrogen-Bonding Ability (∂_h)

	$\Delta f'$	∂_h	λ^{max}_{LE1}, τ_{LE1}	λ^{max}_{LE2}, τ_{LE2}	λ^{max}_{CT1}, τ_{CT1}	λ^{max}_{CT2}, τ_{CT2}
aprotic solvents						
cyclohexane	0.101	0.2			404.6 nm, 0.2 ns	418.6 nm, 0.8 ns
toluene	0.126	2.0			408.8 nm, 1.3 ns	422.8 nm, 2.2 ns
acetonitrile	0.394	6.1			443.5 nm, 2.1 ns	459.3 nm, 3.4 ns
protic solvents						
cyclohexanol	0.343	13.5	433.7 nm, 0.4 ns	452.4 nm, 3.4 ns	468.8 nm, 1.5 ns	483.3 nm, 4.3 ns
1-butanol	0.362	15.8	444.9 nm, ≤0.1 ns		470.2 nm, 0.5 ns	482.2 nm, 3.4 ns
ethanol	0.379	19.4	445.0 nm, ≤0.1 ns		477.5 nm, ≥3.2 ns	501.9 nm, 1.2 ns
water	0.405	42.3			518.1nm, 0.3 ns	533.9 nm, 1.0 ns

in the same wavelength range as those in low polarity protic microenvironments, distorting the correlation between PRODAN emission wavelength and medium properties. Conclusions drawn regarding the polarity of PRODAN binding sites without explicit consideration of hydrogen bonding should be considered carefully in light of these findings.

Conclusions

Time-resolved emission decay matrices (TR-EDMs), also called wavelength dependent emission decays or time-resolved fluorescence spectra, of PRODAN in several protic and aprotic solvents were collected and analyzed using multivariate methods. In all the solvents investigated, PRODAN emits from two states that exhibit charge transfer character. The emission components are separated by approximately 15 nm in emission maxima and approximately 1 ns in decay time. In the alcohols, short-lived, polarity-independent blue bands were resolved from the emission in addition to the charge transfer bands. In one case, cyclohexanol, two blue emission components are separated by approximately 15 nm in emission maxima and approximately 4 ns in decay time. In the others, a single blue band is observed. Interestingly, the red-shifted charge transfer band energies scale with the solvent hydrogen-bonding ability rather than solvent polarizability in the protic solvents. The dependence of the blue bands' photokinetics on the solvent hydrogen-bonding ability suggests that these species are in equilibrium with and/or converted to red-shifted, protonated species. The spectral heterogeneity observed in isotropic solvents suggest that correlating PRODAN emission maxima to the microenvironment properties of some heterogeneous media may require more effort than previously appreciated.

Acknowledgment. Parts of this work were supported by the National Science Foundation (CHE-9983558). The authors thank Paula Falen and Prof. John Koh for their technical assistance with the solvents purified for this work. The authors also thank Prof. Alexander Demchenko for thought provoking discussions on the photokinetics and photochemistry of multistate probes.

Supporting Information Available: More detailed descriptions of the data analysis and quantum chemistry calculations are available as Supporting Information. This material is available free of charge via the Internet at http://pubs.acs.org.

References and Notes

(1) Weber, G.; Farris, F. J. *Biochemistry* **1979**, *18*, 3075.
(2) Valeur, B. *Molecular Fluorescence: Principles and Applicatons*; Wiley-VCH Verlag: Weinheim, Germany, 2002.
(3) Kamal, J. K. A.; Zhao, L.; Zewail, A. H. *Proc. Natl. Acad. Sci. U. S. A.* **2004**, *101*, 13411.
(4) Moreno, F.; Cortijo, M.; Gonzalez-Jimenez, J. *Photochem. Photobiol.* **1999**, *69*, 8.
(5) Massey, J. B.; She, H. S.; Pownall, H. J. *Biochemistry* **1985**, *24*, 6973.
(6) Sommer, A.; Paltauf, F.; Hermetter, A. *Biochemistry* **1990**, *29*, 11134.
(7) Rottenberg, H. *Biochemisty* **1992**, *31*, 9473.
(8) Parasassi, T.; Di Stefano, M.; Loiero, M.; Ravagnan, G.; Gratton, E. *Biophys. J.* **1994**, *66*, 120.
(9) Parasassi, T.; Giusti, A. M.; Gratton, E.; Monoco, E.; Raimondi, M.; Ravagnan, G.; Sapora, O. *Int. J. Rad. Biol* **1994**, *65*, 329.
(10) Bondar, O. P.; Rowe, E. S. *Biophys. J.* **1999**, *76*, 956.
(11) Krasnowska, E. K.; Bagatolli, L. A.; Gratton, E.; Parasassi, T. *Biochim. Biophys. Acta* **2001**, *1511*, 330.
(12) Sengupta, B.; Guharay, J.; Sengupta, P. K. *Spectrochim. Acta, Part A* **2000**, *56*, 1433.
(13) Hutterer, R.; Hof, M. *J. Fluorescence* **2001**, *11*, 227.
(14) Sykora, J.; Jurkiewicz, P.; Epand, R. M.; Kraayenhof, R.; Langner, M.; Hof, M. *Chem. Phys. Lipids* **2005**, *135*, 213.
(15) Wilson-Ashworth, H. A.; Bahm, Q.; Erickson, J.; Shinkle, A.; Vu, M. P.; Woodbury, D.; Bell, J. D. *Biophys. J.* **2006**, *91*, 4091.
(16) Parusel, A. B. J.; Schneider, F. W.; Kohler, G. *J. Mol. Struct.* **1997**, *398−399*, 341.
(17) Parusel, A. B. J. *J. Chem. Soc., Faraday Trans.* **1998**, *94*, 2923.
(18) Parusel, A. B. J.; Nowak, W.; Grimme, S.; Kohler, G. *J. Phys. Chem. A* **1998**, *102*, 7149.
(19) Ilich, P.; Prendergast, F. G. *J. Phys. Chem.* **1989**, *93*, 4441.
(20) Samanta, A.; Fessenden, R. *J. Phys. Chem. A* **2000**, *104*, 8972.
(21) Lobo, B. C.; Abelt, C. J. *J. Phys. Chem. A* **2003**, *107*, 10938.
(22) Davis, B. N.; Abelt, C. J. *J. Phys. Chem. A* **2005**, *109*, 1295.
(23) Mennucci, B.; Caricato, M.; Ingrosso, F.; Cappelli, C.; Cammi, R.; Tomasi, J.; Scalmani, G.; Frisch, M. J. *J. Phys. Chem. B* **2008**, *112*, 414.
(24) Bakshiev, G. N. *Opt. Spectrosc.* **1964**, *16*, 446.
(25) Heisel, F.; Miehe, J. A.; Szemik, A. W. *Chem. Phys. Lett.* **1987**, *138*, 321.
(26) Zurawsky, W.; Scarlata, S. *J. Phys. Chem.* **1992**, *96*, 6012.
(27) Catalan, J.; Perez, P.; Laynez, J.; Blanco, F. G. *J. Fluorescence* **1991**, *1*, 215.
(28) Chapman, C. F.; Fee, R. S.; Maroncelli, M. *J. Phys. Chem.* **1995**, *99*, 4811.
(29) Viard, M.; Gallay, J.; Vincent, M.; Meyer, O.; Robert, B.; Paternostre, M. *Biophys. J.* **1997**, *73*, 2221.
(30) Artyukhov, V. Y.; Zharkova, O. M.; Morozova, Y. P. *J. Appl. Spectrosc.* **2005**, *72*, 349.
(31) Perrin, C. L.; Nielson, J. B. *Annu. Rev. Phys. Chem.* **1997**, *48*, 511.
(32) Balter, A.; Nowak, W.; Pawelkiewicz, W.; Kowalczyk, A. *Chem. Phys. Lett.* **1988**, *143*, 565.
(33) Baumann, J.; Calzaferri, G.; Forss, L.; Hugentobler, T. *J. Photochem.* **1985**, *28*, 457.
(34) Beechem, J. M.; Brand, L. *Annu. Rev. Biochem.* **1985**, *54*, 43.
(35) Windig, W.; Guilment, J. *Anal. Chem.* **1991**, *63*, 1425.
(36) Jiang, J. H.; Ozaki, Y. *Appl. Spectrosc. Rev.* **2002**, *37*, 321.
(37) Zimanyi, L.; Saltiel, J.; Brown, L. S.; Lanyi, J. K. *J. Phys. Chem. A* **2006**, *110*, 2318.
(38) Fox, C. B.; Uibel, R. H.; Harris, J. M. *J. Phys. Chem. B* **2007**, *111*, 11428.
(39) Strang, G. *Linear Algebra and Its Applications*, 3rd ed.; Harcourt Brace Jovanovich, Publishers: San Diego, CA, 1988.
(40) Wold, S. *Technometrics* **1978**, *20*, 397.
(41) Malinowski, E. R. *Factor Analysis in Chemistry*, 2nd ed.; Wiley: New York, 1991.
(42) Shrager, R. I.; Hendley, R. W. *Anal. Chem.* **1982**, *54*, 1147.
(43) Rossi, T. M.; Warner, I. M. *Anal. Chem.* **1986**, *58*, 810.
(44) Faber, K.; Kowalski, B. R. *J. Chemom.* **1997**, *11*, 53.
(45) Beechem, J. M.; Gratton, E.; Ameloot, M.; Knutson, J. R.; Brand, L. The global analysis of fluorescence intensity and anisotropy decay data: second-generation theory and programs. In *Topics in Fluorescence Spectroscopy*; Lakowicz, J. R., Ed.; Plenum: New York, 1991; Vol. 2, p 241.
(46) Ameloot, M.; Boens, N.; Andriessen, R.; Van den Bergh, V.; De Schryver, F. C. *J. Phys. Chem.* **1991**, *95*, 2041.
(47) Windig, W.; Antalek, B. *Chemom. Intell. Lab. Syst.* **1997**, *37*, 241.
(48) Windig, W.; Antalek, B.; Robbins, M. J.; Zumbulyadis, N.; Heckler, C. E. *J. Chemom.* **2000**, *14*, 213.
(49) Livesey, A. K.; Brochon, J. C. *Biophys. J.* **1987**, *52*, 693.
(50) Brochon, J.-C.; Livesey, A. K. *Biophys. J.* **1987**, *52*, 693.
(51) Neal, S. L.; Davidson, E. R.; Warner, I. M. *Anal. Chem.* **1990**, *62*, 658.
(52) Neal, S. L. *J. Phys. Chem. A* **1997**, *101*, 6883.
(53) Paatero, P.; Tapper, U. *Environmetrics* **1994**, *5*, 111.
(54) Van Benthem, M. H.; Keenan, M. R.; Haaland, D. M. *J. Chemom.* **2002**, *16*, 613.
(55) Frisch, M. J., et al. Gaussian 03, revision B.05 (SGI64-G03RevB.05); Gaussian, Inc.: Wallingford, CT, 2004.
(56) Schlegel, H. B. *J. Comput. Chem.* **1982**, *3*, 214.
(57) Dooley, R.; Milfeld, K.; Guiang, C.; Pamidighantam, S.; Allen, G. *J. Grid Comput.* **2006**, *4*, 195.
(58) Becke, A. D. *Phys. Rev. A* **1988**, *38*, 3098.
(59) Lee, C. T.; Yang, W. T.; Parr, R. G. *Phys. Rev. B* **1988**, *37* 785.
(60) Zhao, Y.; Truhlar, D. G. *J. Phys. Chem. A* **2004**, *108*, 6908.
(61) Hehre, W. J.; Radom, L.; Schleyer, P. v. R.; Pople, J. A. *Ab Initio Molecular Orbital Theory*; Wiley: New York, 1986.
(62) Bauernschmitt, R.; Ahlrichs, R. *Chem. Phys. Lett.* **1996**, *256* 454.
(63) Casida, M. E.; Jamorski, C.; Casida, K. C.; Salahub, D. R. *J. Chem. Phys.* **1998**, *108*, 4439.
(64) Stratmann, R. E.; Scuseria, G. E.; Frisch, M. J. *J. Chem. Phys.* **1998**, *109*, 8218.
(65) Klamt, A.; Schuurmann, G. *J. Chem. Soc., Perkin Trans. 2* **1993**, 799.

(66) Barone, V.; Cossi, M.; Tomasi, J. *J. Comput. Chem.* **1998**, *19*, 404.

(67) Artyukhov, V. Y.; Zharkova, O. M.; Morozova, Y. P. *Russ. Phys. J.* **2004**, *47*, 1172.

(68) Parasassi, T.; De Stasio, G.; Ravagnan, G.; Rusch, R. M.; Gratton, E. *Biophys. J.* **1991**, *60*, 179.

(69) Barton, A. F. M. *Handbook of Solubility Parameters*; CRC Press: Boca Raton, FL, 1983.

(70) Krystkowiak, E.; Dobek, K.; Maciejewski, A. *J. Photochem. Photobiol. A* **2006**, *184*, 250.

(71) Sengupta, P. K.; Kasha, M. *Chem. Phys. Lett.* **1979**, *68*, 382.

(72) Klymchenko, A. S.; Duportail, G.; Demchenko, A. P.; Mely, Y. *Biophys. J.* **2004**, *86*, 2929.

(73) Chen, Y.; Topp, M. R. *Chem. Phys. Lett.* **2002**, *355*, 270.

(74) Cser, A.; Nagy, K.; Biczok, L. *Chem. Phys. Lett.* **2002**, *360*, 473.

JP802260Y